Pis'ma v ZhETF, vol. 102, iss. 6, pp. 405 – 409

Measurements of weak localization of graphene in inhomogeneous magnetic fields

N. Lindvall[+1)], *A. Shivayogimath*[*], *A. Yurgens*[+]

[+]*Chalmers University of Technology/MC2, SE-41296 Gothenburg, Sweden*

[*]*DTU Nanotech – Technical University of Denmark, DK-2800 Kgs. Lyngby, Denmark*

Submitted 1 June 2015 2015

Resubmitted 16 July 2015

Weak localization in graphene is studied in inhomogeneous magnetic fields. To generate the inhomogeneous field, a thin film of type-II superconducting niobium is put in close proximity to graphene. A deviation from the ordinary quadratic weak localization behavior is observed at low fields. We attribute this to the inhomogeneous field caused by vortices in the superconductor. The deviation, which depends on the carrier concentration in graphene, can be tuned by the gate voltage. In addition, collective vortex motion, known as vortex avalanches, is observed through magnetoresistance measurements of graphene.

DOI: 10.7868/S0370274X15180095

Graphene is an intensively studied two-dimensional material consisting of a single layer of sp^2-hybridized carbon atoms. It exhibits extraordinary mechanical and electrical properties [1, 2], making it interesting both for fundamental studies and potential applications [3, 4]. The electronic properties of graphene in magnetic fields have been of particular interest. In most cases, weak localization (WL) dominates the magnetoresistance of graphene at low magnetic fields. Many properties, including the charge carrier mobility and various scattering lengths, can be deduced from such measurements. Weak localization has been widely studied in graphene produced by a range of different methods [5–7]. These studies consider graphene in a homogeneous magnetic field. In this work, we extend the study of graphene WL to inhomogeneous magnetic fields.

Weak localization in inhomogeneous magnetic fields has been studied for traditional 2D electron gases (2DEGs), both theoretically [8, 9] and experimentally [10–13]. To produce the inhomogeneous field, a type-II superconducting thin film is put in close vicinity of, but electrically separated from, the 2DEG. This was realized by changing the ordinary metal gate in 2DEG metal–oxide–semiconductor field-effect transistors (MOSFETs) to a type-II superconductor. Quanta of magnetic flux penetrate the superconducting film at various locations, creating a spatially inhomogeneous magnetic field close to the surface of the superconductor. The WL correction to the conductivity at low magnetic fields is qualitatively different in the case of inhomogeneous fields, yielding a linear dependence of conductivity on magnetic field, instead of the classical quadratic behavior. This device geometry allows studies of WL in graphene in inhomogeneous magnetic fields including the possibility of tuning scattering lengths by changing the charge carrier density.

To model WL in graphene in *homogenous* magnetic fields, we follow the theory in Ref. [14] which has proven valid for a wide range of graphene samples [5]. The conductivity σ as a function of the magnetic field B is modeled as:

$$\sigma(B) = \sigma(0) + \Delta\sigma(B) = \sigma(0) + \\ + \frac{e^2}{\pi h}\left[F\left(\frac{B}{B_\varphi}\right) - F\left(\frac{B}{B_\varphi + 2B_i}\right) - 2F\left(\frac{B}{B_\varphi + B_*}\right)\right], \quad (1)$$

where e is the elementary charge, h is the Planck constant, $F(z) = \ln(z) + \Psi(0.5 + z^{-1})$, Ψ is the digamma function, $B_{\varphi,i,*} = h/(8\pi e L^2_{\varphi,i,*})$ are the characteristic fields from which the characteristic lengths $L_{\varphi,i,*}$ can be derived. The phase coherence length L_φ corresponds to inelastic scattering and $L_{i,*}$ are the elastic scattering lengths. Characteristic fields $B_{\varphi,i,*}$ are used as fitting parameters. For small fields, the WL behavior of graphene is quadratic, similar to ordinary 2DEGs.

There has been little theoretical work on graphene WL in *inhomogeneous* fields [15–17]. For ordinary 2DEGs, inhomogeneous WL was studied in the case of cylindrical flux tubes with radius r_0 smaller than L_φ. In such a case, the WL correction to the conductivity for low fields is linear instead of parabolic. If the mutual

[1)]e-mail: niclas.lindvall@chalmers.se

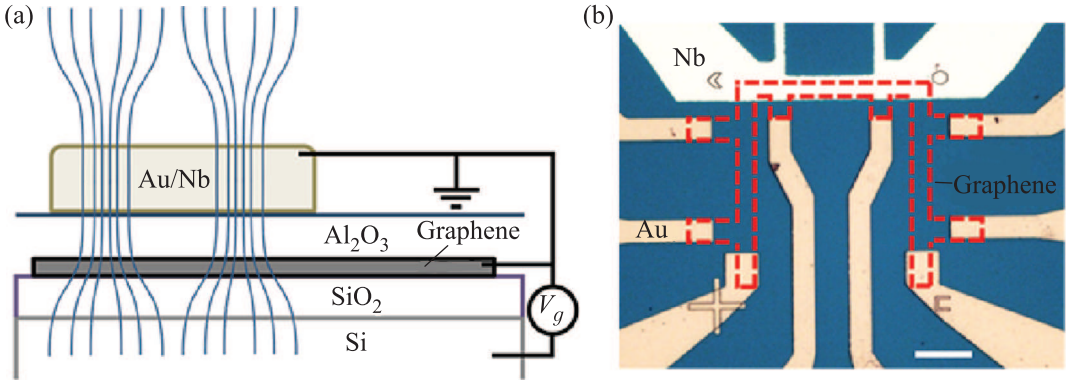

Fig. 1. (Color online) (a) – Side view schematics of the sample layout. The magnetic field penetrates Nb in form of vortices, shown in blue. (b) – Optical image of the actual device seen from the top. The graphene is highlighted in red. The design allows for four-probe resistance measurements of both uncovered- and Nb-covered areas of the graphene. The scale-bar is 20 μm

separation of flux tubes is larger than L_φ, the conductivity correction can be written as [8]:

$$\Delta\sigma = \frac{e^2}{\pi h}\frac{1}{\ln(b_0/B_\varphi)}\left(\frac{|B|}{B_\varphi}\right), \qquad (2)$$

where b_0 is the magnitude of the magnetic field inside the tubes. This is valid until B is greater than B_φ where the ordinary WL result is recovered.

Graphene grown on copper by chemical vapor deposition (CVD) is transferred to standard SiO_2 (290 nm)/Si(n++) substrates [18]. Chemical vapor deposition grown graphene is used in order to obtain large-area graphene with a reasonably long L_φ. A too long L_φ means that the magnetic fields, at which inhomogeneity of the field would matter, are low and difficult to measure at. The conducting silicon substrate serves as a back gate electrode. In two subsequent electron-beam lithography (EBL) steps, graphene and electrodes are patterned using oxygen plasma etching and lift-off of Au (80 nm)/Ti (3 nm) thin film, respectively. 30 nm of Al_2O_3 is deposited using atomic layer deposition (ALD) following a nucleation step where 2 nm of aluminum is deposited by evaporation and subsequently oxidized for 5 min at 200 °C in ambient atmosphere. Then, 40 nm of Nb is deposited by sputtering followed by the evaporation of Au (50 nm)/Ti (3 nm) to facilitate wire bonding. In the final EBL step, selective areas of the Au/Nb film are removed using argon-ion- and NF_3 reactive-ion etching. A side-view schematic of the device is shown in Fig. 1a. It is essentially a double-gate field-effect graphene transistor with a superconducting top gate. Fig. 1b shows an optical image of the device. The design offers the possibility of four-probe resistance measurements of Nb and both uncovered- and Nb-covered graphene. Graphene resistance is measured over a $W \times L = 8 \times 32\,\mu\text{m}^2$ area. We have also tested devices where an unpatterned Nb thin film instead was placed under graphene, showing essentially the same results.

Four-probe resistance measurements are performed in a dipstick immersed in liquid He at 4 K using a low-frequency lock-in technique with a typical current of 250 nA. The magnetic field is perpendicular to graphene and the Nb thin film. Due to strong vortex pinning in Nb, a certain increase in magnetic field is needed for the vortices to move into interior of the thin film. They do so in a collective manner in the form of vortex avalanches [19, 20]. This leads to a step-wise change of the effective magnetic field close to the superconducting film. While this is interesting in its own right, it makes WL measurements difficult [12]. To avoid the vortex avalanches and the screening of the magnetic field by the Meissner effect, a field-cooling technique is used [11, 12]. First, the sample is heated above the critical temperature of Nb and the magnetic field is set. Then, the sample is cooled to base temperature in constant magnetic field. Finally, the resistance is measured. While in principle this procedure is only necessary for Nb-covered graphene, the data presented here for uncovered graphene are measured in the same way for comparison.

Fig. 2a shows weak localization measurements of Nb-covered graphene with a back gate voltage of $V_g = -20$ V. The graphene is intrinsically n-doped after fabrication. It remains n-doped for the full range of gate voltages applied. The measurement has been averaged over four magnetic field sweeps. For a wide range of $|B| > 3$ mT the data is well described by the ordinary graphene WL theory, which allows us to estimate the scattering lengths using Eq. (1). For small fields, however, a deviation from the theory is observed.

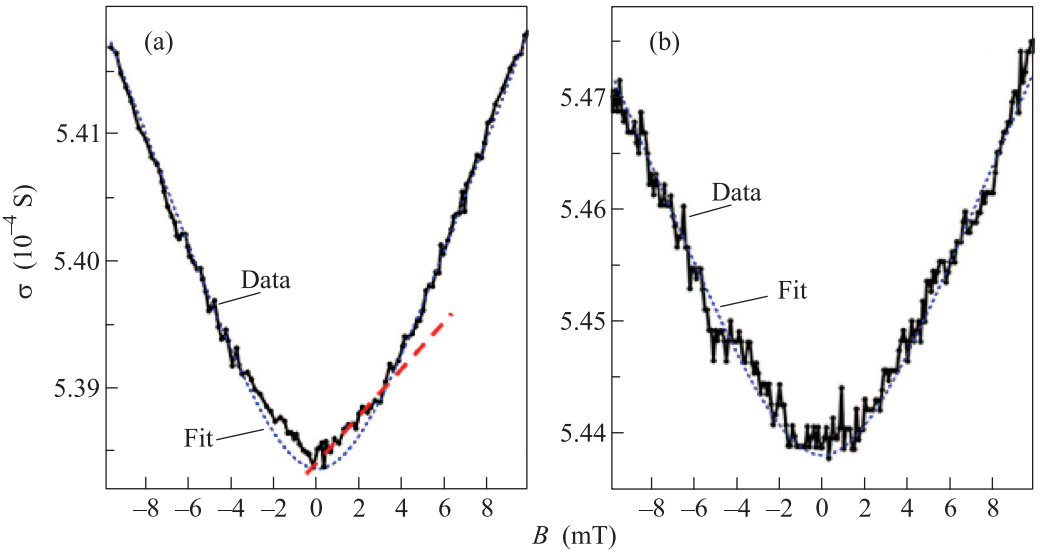

Fig. 2. (Color online) (a) – Weak localization measurements of graphene under Nb subject to inhomogeneous magnetic fields. For $B < 3$ mT it shows a deviation from the ordinary quadratic behavior. The fitting parameters obtained from Eq. 1 are $B_\varphi = 2.6$ mT ($L_\varphi = 250$ nm), $B_i = 200$ mT ($L_i = 29$ nm), and $B_* = 500$ mT ($L_* = 18$ nm). The gate voltage is $V_g = -20$ V. (b) – Similar measurement for uncovered graphene not subject to inhomogeneous magnetic fields with similar conductance and L_φ. The fitting parameters are $B_\varphi = 2.8$ mT ($L_\varphi = 240$ nm), $B_i = 670$ mT ($L_i = 16$ mn), and $B_* = 800$ mT ($L_* = 14$ nm). The gate voltage is $V_g = +15$ V. The measurements in both a and b are made using field cooling to 4 K

Fitting using Eq. (1) gives $B_\varphi = 2.6$ mT ($L_\varphi = 250$ nm) which roughly corresponds to the region of the non-standard behavior. The obtained elastic scattering terms yield $B_i = 200$ mT ($L_i = 29$ nm) and $B_* = 500$ mT ($L_* = 18$ nm). As noted previously by Baker et al. [5], it can be difficult to ascertain accurate values for these two scattering terms due to the degree in which the two are mathematically convoluted in Eq. (1). Elastic scattering dominates over inelastic processes in all samples measured, which is typical for graphene, and the values for the more robust fitting parameter L_φ are similar to those previously reported for CVD-grown graphene [5].

A similar measurement, but performed using only one single sweep, of uncovered graphene (no Nb on top) with comparable conductance and L_φ is shown in Fig. 2b for comparison. The data can be well described by Eq. (1) as expected. For uncovered graphene, measurements of WL with and without the field-cooling procedure yield similar results.

The possibility to tune L_φ by changing the carrier concentration offers an interesting possibility for WL studies in graphene. Fig. 3 shows WL measurements of Nb-covered graphene for four different gate voltages: $V_g = -20$, -15, 0, and $+15$ V. Value L_φ increases from $L_\varphi = 250$ nm ($B_\varphi = 2.6$ mT) for $V_g = -20$ V to $L_\varphi = 320$ nm ($B_\varphi = 1.6$ mT) for $V_g = +15$ V. For the negative gate voltages, one can see a deviation from quadratic dependence. The anomalous behavior decreases with increasing V_g (and increasing L_φ), eventually vanishing for $V_g = +15$ V.

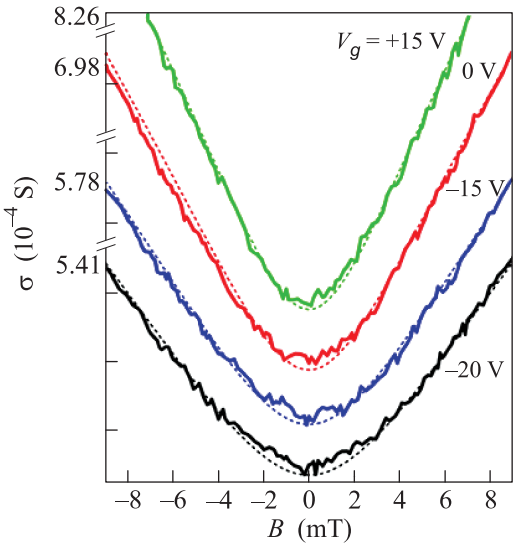

Fig. 3. (Color online) Weak localization of Nb-covered graphene for $V_g = -20$, -15, 0, and $+15$ V, respectively (arbitrarily shifted along the y-axis). The graphene is n-doped for all four cases. The carrier concentration is increased from the bottom to the top curve, and correspondingly L_φ increases from 250 to 322 nm. The effect of inhomogeneous field becomes less visible for increasing V_g. All measurements are performed using field cooling to 4 K

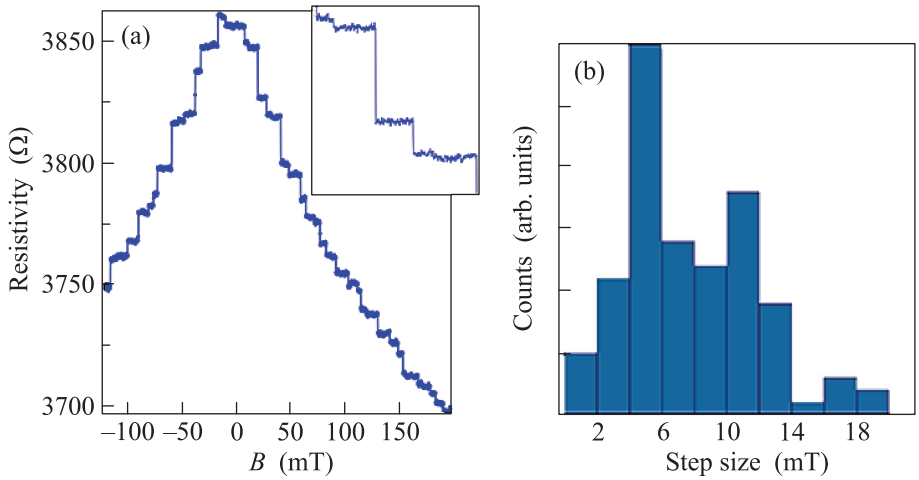

Fig. 4. (Color online) (a) – Weak localization in Nb-covered graphene cooled down to 4 K in zero field and $V_g = 0$ V. The resistance changes stepwise, revealing vortex avalanches in Nb. The inset shows a magnification of the resistance steps. (b) – Histogram of the magnetic step width, revealing a typical step size of about 5 mT

While we observe a deviation from homogeneous WL graphene theory for Nb-covered samples, the effect is weak and our measurement precision does not allow us to quantify our results, for example by fitting the data using Eq. (2). Quantification of the results was problematic also in previous measurements on 2DEGs in inhomogeneous fields, despite displaying a larger deviation from quadratic WL behavior [9, 10]. In our samples the deviation is seen for $|B| \lesssim B_\varphi$, in qualitative agreement with the theoretical findings of Rammer et al. [8]. Other theories assume ballistic transport in inhomogeneous fields [12, 13], where the mean free path l_m is larger than the separation between vortices. These are not applicable to our samples, which are in the diffusive regime with an estimated $l_m \ll 100$ nm from the Drude conductivity. Moreover, the positive magnetoresistance associated with these theories is not replicated here, ruling out their relevance to our findings.

While we find qualitative agreement between our results and that obtained on 2DEGs, the additional contribution of elastic scattering processes to the WL characteristics in graphene may make the situation unique in this case. In this regard, the randomly modulated magnetic field introduced by the underlying flux lattice in the vicinity of the graphene could induce field-dependent contributions to intravalley scattering, thereby leading to an increased intravalley scattering at fields where the inhomogeneity of the field is significant. This would lead to a field-dependent attenuation of WL at low fields, similar to the effect of pseudomagnetic fields seen for graphene flakes [6, 21]. However, the elastic length scales are roughly one order of magnitude shorter than the phase coherence length and hence much shorter than the average distance between vortices. Despite the discrepancy in length scales, we cannot presently rule out that elastic scattering has an effect on the low-field WL of graphene.

Weak localization magnetoresistance allows for the detection of vortex avalanches. This is done by omitting the field-cooling measurement procedure described previously and instead directly sweeping the magnetic field at 4 K. The resistance changes step-wise instead of continuously, thus revealing the vortex avalanches. While observed in all Nb-covered graphene samples, this effect is more pronounced when the Nb is unpatterned underneath graphene, covering the full 6-mm extent of the substrate. Fig. 4a shows such WL-magnetoresistance measurements. The resistance changes with the magnetic field in steps. These resistance steps are always present at low temperature but their position in magnetic field is not reproducible. Fig. 4b shows a histogram of step sizes in B, with typical values around 5 mT.

In conclusion we have measured weak localization in graphene in inhomogeneous magnetic fields by putting it in close proximity to a superconducting thin film. For small fields there is a deviation from the typical quadratic WL behavior, which is not observed for non Nb-covered graphene reference devices. We attribute this to the inhomogeneous nature of the field similar to what has been observed in ordinary 2DEGs. The effect is weaker than what has been observed for 2DEGs. One possible explanation is the macroscopic inhomogeneity of the samples, but it could also stem from the elastic scattering contributions to WL in graphene. By changing the gate voltage the phase coherence length can be tuned and for large L_φ the effect vanishes. Finally, we

have used WL in graphene to reveal vortex avalanches in Nb, similar to what has been observed previously using other techniques.

1. A. S. Mayorov, R. V. Gorbachev, S. V. Morozov, L. Britnell, R. Jalil, L. A. Ponomarenko, P. Blake, K. S. Novoselov, K. Watanabe, T. Taniguchi, and A. K. Geim, Nano. Lett. **11**, 2396 (2011).
2. Y. B. Zhang, Y. W. Tan, H. L. Stormer, and P. Kim, Nature **438**, 201 (2005).
3. K. S. Novoselov, V. I. Falko, L. Colombo, P. R. Gellert, M. G. Schwab, and K. Kim, Nature **490**, 192 (2012).
4. A. K. Geim and K. S. Novoselov, Nat. Mater. **6**, 183 (2007).
5. A. M. R. Baker, J. A. Alexander-Webber, T. Altebaeumer, T. J. B. M. Janssen, A. Tzalenchuk, S. Lara-Avila, S. Kubatkin, R. Yakimova, C. T. Lin, L. J. Li, and R. J. Nicholas, Phys. Rev. B **86**, (2012).
6. F. V. Tikhonenko, D. W. Horsell, R. V. Gorbachev, and A. K. Savchenko, Phys. Rev. Lett. **100**, (2008).
7. F. V. Tikhonenko, A. A. Kozikov, A. K. Savchenko, and R. V. Gorbachev, Phys. Rev. Lett. **103**, (2009).
8. J. Rammer and A. L. Shelankov, Phys. Rev. B **36**, 3135 (1987).
9. G. H. Li, M. Wang, G. L. Liu, S. T. Liu, S. G. Wang, and S. S. Yan, Chinese Phys. Lett. **12**, 621 (1995).
10. S. J. Bending, K. von Klitzing, and K. Ploog, Phys. Rev. Lett. **65**, 1060 (1990).
11. A. K. Geim, JETP Lett. **50**, 389 (1989).
12. A. K. Geim, S. J. Bending, I. V. Grigorieva, and M. G. Blamire, Phys. Rev. B **49**, 5749 (1994).
13. A. Smith, R. Taboryski, L. T. Hansen, C. B. Sorensen, P. Hedegard, and P. E. Lindelof, Phys. Rev. B **50**, 14726 (1994).
14. E. McCann, K. Kechedzhi, V. I. Fal'ko, H. Suzuura, T. Ando, and B. L. Altshuler, Phys. Rev. Lett. **97**, (2006).
15. M. R. Masir and F. M. Peeters, J. Comput. Electron. **12**, 115 (2013).
16. M. R. Masir, P. Vasilopoulos, and F. M. Peeters, J. Phys. Cond. Mat. **23**, (2011).
17. P. Roy, T. K. Ghosh, and K. Bhattacharya, J. Phys. Cond. Mat. **24**, (2012).
18. J. Sun, N. Lindvall, M. Cole, K. Angel, T. Wang, K. Teo, D. Chua, J. Liu, and A. Yurgens, IEEE Trans. Nanotechnol. **11**, 255 (2012).
19. E. Altshuler and T. H. Johansen, Rev. Mod. Phys. **76**, 471 (2004).
20. M. S. Welling, R. J. Westerwaal, W. Lohstroh, and R. J. Wijngaarden, Physica C **411**, 11 (2004).
21. S. V. Morozov, K. S. Novoselov, M. I. Katsnelson, F. Schedin, L. A. Ponomarenko, D. Jiang, and A. K. Geim, Phys. Rev. Lett. **97**, (2006).